IEEE Access
Multidisciplinary | Rapid Review | Open Access Journal

Received 12 March 2024, accepted 10 April 2024, date of publication 15 April 2024, date of current version 26 April 2024.

Digital Object Identifier 10.1109/ACCESS.2024.3389495

RESEARCH ARTICLE

FBG Sensor for Heart Rate Monitoring Using 3D Printing Technology

M. FAJKUS[1], M. KOSTELANSKY[1], M. FRIDRICH[1], J. CUBIK[1], S. KEPAK[1], D. KRIZAN[1], R. MARTINEK[2], (Senior Member, IEEE), MAZIN ABED MOHAMMED[1,2,3], AND J. NEDOMA[1], (Senior Member, IEEE)

[1]Department of Telecommunications, Faculty of Electrical Engineering and Computer Science, VSB—Technical University of Ostrava, 70800 Ostrava, Czech Republic
[2]Department of Cybernetics and Biomedical Engineering, Faculty of Electrical Engineering and Computer Science, VSB—Technical University of Ostrava, 70800 Ostrava, Czech Republic
[3]Department of Artificial Intelligence, College of Computer Science and Information Technology, University of Anbar, Anbar 31001, Iraq

Corresponding author: M. Fajkus (marcel.fajkus@vsb.cz)

This work was supported in part by the European Union through the REFRESH—Research Excellence For REgion Sustainability and High-tech Industries under Project CZ.10.03.01/00/22_003/0000048 via the Operational Program Just Transition; and in part by the Ministry of Education, Youth and Sports of the Czech Republic conducted by the VSB—Technical University of Ostrava under Grant SP2024/081.

This work involved human subjects or animals in its research. Approval of all ethical and experimental procedures and protocols was granted by the Ethics Commission at VSB-TU Ostrava under Application No. VSB/23/109812.

ABSTRACT Currently, the use of fiber-optic Bragg gratings in biomedical applications, especially in the field of magnetic resonance imaging (MRI), is becoming popular. In these applications, the fiber Bragg grating (FBG) encapsulation plays a crucial role in terms of the accuracy and reproducibility of the measurements. This paper describes in detail the fabrication method of a prototype FBG sensor, which is realized by encapsulating a Bragg grating between two layers of the MR-compatible material Acrylonitrile Butadiene Styrene (ABS) by 3D printing. The sensor thus created, implemented, for example, on the chest of a human body, enables monitoring of the vital functions of the human body. The paper describes the complete procedure for the creation of the prototype sensor, including strain and temperature dependence, as well as results of long-term experimental measurements against the conventional electrocardiography (ECG) standard. Results based on the objective Bland-Altman (B-A) method confirm that the implemented sensor can be used for reliable monitoring of cardiac activity (>95% based on B-A). Taking into account the single fiber optic cable, its simple implementation, its small size and weight < 5g, the presented sensor represents an interesting alternative to conventional ECG.

INDEX TERMS Fibre Bragg grating, 3D printing, vital sign monitoring, heart rate, MR-compatible.

I. INTRODUCTION

Monitoring cardiac activity is a key element in the diagnosis and tracking of the health status of patients. Heart rate and its variability provide valuable information on heart function and the general condition of the cardiovascular system. Electrocardiography (ECG) is a standard and widely used method to record electrical activity of the heart, which allows the identification of potential arrhythmias, ischemia, or other abnormalities. ECG records the electrical activity of the heart, resulting in an electrocardiogram containing a sequence of PQRST waves [1], [2]. A very specific environment is magnetic resonance imaging, which uses strong magnetic fields to create detailed images of the internal organs and structures of the human body. In some cases, cardiac activity monitoring is used during magnetic resonance imaging. These cases include the investigation of patients with heart disease or high-risk conditions

The associate editor coordinating the review of this manuscript and approving it for publication was Salvatore Surdo.

(e.g., a patient with a pacemaker), but also in the case of imaging the heart itself, where it is necessary to synchronize the imaging with the activity of the heart to achieve sharp and clear images.

The standard method for monitoring cardiac activity in an MRI environment is an MR-compatible ECG [3]. However, these lead to the problem of the magnetohydrodynamic principle of electrically conducting blood, whose electric current is added to the cardiac signal, increasing the t-wave amplitude in the MR environment. This overshoot of the QRS complex causes inaccurate synchronization, leading to less sharp images and prolonged examinations [4]. Alternatives to MR-compatible ECG are methods such as photoplethysmography [5] or acoustic systems [6], which are fully immune to electromagnetic fields. In addition to monitoring cardiac activity in the MR environment, respiratory monitoring is also performed, where the tunnel environment can cause hyperventilation due to the shortness of breath (dyspnea) [7].

The above-mentioned conventional approaches are used to monitor fundamental parameters of the human body in long-term or intensive care units, sleep laboratories, or MRI environments. An alternative approach is fiber optic technology, which is immune to electromagnetic interference, has a very small footprint, and can be operated with a single lead optical cable.

The first group is represented by intensity (micro bending) sensors based on the evaluation of changes in the optical power of light passing through optical fibers [8]. Usually, these sensors are placed in the pad on which the patient is lying. During respiration, there is a variable load on the sensor that results in modulation of intensity of the transmitted or reflected light [9].

Another group of fiber-optic sensors uses the principle of light interference. These sensors exhibit high sensitivity in measuring vibration, acceleration, and derived quantities and are found in Mach-Zehnder [10], Michelson [11], Sagnac [12] or Fabry-Perot [13] interferometer arrangements. The Mach-Zehnder-based interferometric approach represents the simplest option for monitoring vital signs of the human body [10]. Due to its high sensitivity, it can record both respiratory and cardiac activity [14].

The third group consists of sensors that use fiber Bragg gratings (FBG) [15], which are the fastest growing fiber optic sensor technology in biomedical applications [16]. These sensors are also sensitive enough to monitor cardiac activity in addition to respiratory activity [17]. The use of FBG sensors in monitoring of respiratory and cardiac activity requires appropriate encapsulation of the Bragg grating, which aims to achieve the required sensitivity to the pressure caused by respiration and cardiac activity and to provide protection against damage. The use of FBG sensors to monitor respiratory and cardiac activity requires appropriate encapsulation of the Bragg grating, which aims to achieve the required sensitivity to pressure caused by respiration and cardiac activity and to provide protection against damage.

The simplest encapsulation methods include the attachment of an optical fiber with a Bragg grating to a flexible plastic pad on which the subject is lying [17]. Increasing the precision of the respiration and heart rate can be achieved by implementing a cascade connection of several Bragg gratings with a single fiber optic cable [18]. Another option is to implement an FBG sensor on the chest in the region of the heart. These sensors consist of a Bragg grating encapsulated typically in polymers (e.g., polydimethylsiloxane PDMS) and fixed with an elastic chest band [19], [20]. Due to their location close to the heart, they exhibit high sensitivity to cardiac activity [21], [22]. An interesting approach involves encapsulating FBG sensors within smart patches for the simultaneous monitoring of respiratory and heart activity. The study demonstrates the high fidelity of the smart patch in estimating heart rate (HR) and respiratory rate (RR) under various respiratory conditions and common daily body positions, while maintaining patient comfort throughout the examination [23]. The most recent approach is to encapsulate Bragg gratings in mattresses, beds [24] and smart textiles [25].

The emerging field of Bragg grating encapsulation uses 3D printing technology. The authors of papers [26], [27], [28], [29], [30], [31] presented experiments on the encapsulation of FBGs in polymer structures. Encapsulation using 3D printing technology was found to not affect the functionality of the FBG or the shape of the reflectance spectrum [30], only the reflectance spectrum is shifted and the sensitivity to mechanical loading is affected. For example, when embedded in a thermoplastic polyurethane (TPU) material, a shift of the reflectance spectrum by 136 pm was observed and also a bending sensitivity of about 1.74× compared to bare fiber with a Bragg grating has been demonstrated [31]. However, the encapsulation material itself has a significant effect on the temperature sensitivity, which can increase more than tenfold [27], [28], [32].

The authors of the paper [33] presented the application of encapsulated FBG sensors using 3D printing technology to monitor structural stresses, presenting a prototype with three Bragg gratings for effective stress change observation. Further analysis revealed that FBG sensors with polyimide-coated fibers encapsulated in Acrylonitrile Butadiene Styrene (ABS) exhibited significantly higher strain sensitivity, approximately 2.5 times greater, compared to those with acrylate protection and Polylactic Acid (PLA) encapsulation. [34]

A more detailed analysis compared, in addition to the above materials, Ormocer primary protection and TPU filament [35]. The temperature loading results show that ABS samples exhibit a temperature sensitivity of approximately 116 pm/°C in the range up to 60 °C, while PLA samples exhibit a temperature sensitivity of up to 139 pm/°C, but cannot be used at temperatures higher than 40 °C. In the case of tensile tests, the highest response was achieved for samples made of TPU filament.

Other applications of sensors based on Bragg gratings encapsulated using 3D printing technology that have been published include pressure sensors [26], tilt sensors with a sensitivity of 10 pm/° [36] or, for example, special clamps for mounting an industrial hydraulic piping system to detect its loosening or determine its natural resonant frequency [37].

Although various studies have explored the use of 3D printing and fiber optic sensors for diverse applications, this publication uniquely focuses on utilizing 3D-printed FBG sensors for vital sign monitoring. Previous works [38] and [39] have explored the measurement of heart and breathing rates with 3D-printed encapsulated Bragg gratings, while [40] employs PLA filament for FBG sensor encapsulation, unlike using the ABS filament described in this article, which has different mechanical properties that affect sensor performance. Additionally, such FBG sensors have been applied in biomedical devices such as spirometers [41] and respiratory activity sensors embedded in oxygen masks [42], offering advantages in MRI environments by reducing motion artifacts.

In [43], a thumb-shaped FBG sensor encapsulated with Fused Deposition Modeling (FDM) technology was developed for use under an anesthesiologist's glove to precisely locate the epidural space. The optical signal changes when the needle contacts the epidural space, helping anesthesiologists in real-time needle positioning to improve procedure success rates.

Table 1 compares the method of encapsulating Bragg gratings using 3D printing technology and its effect on temperature and strain sensitivity as a function of filament type. The results show that, for example, the resulting temperature sensitivity is not only influenced by the filament type itself, but also by the specific filament composition or by the dimensions and method of imprinting.

TABLE 1. Comparison of strain and temperature sensitivities of FBGs encapsulated using 3D printing technology.

Measurand	Sensitivity	Filament	Reference
Temperature	112.3 pm/°C	PLA	[6]
Temperature	30-40 pm/°C	PLA	[28]
Temperature	94.5 pm/°C	ABS	[6]
Temperature	44.5 pm/°C (sensor 1) 105.3 pm/°C (sensor 2)	ABS	[27]
Temperature	19.2 pm/°C	TPU	[31]
Temperature	9,4 pm/°C	Photopolymer	[27]
Deformation	0.38 pm/μstrain	PLA	[28]
Deformation	0.71 a 0.76 pm/μstrain	Not specified	[30]

The above review shows a number of advantages of fiber optic Bragg gratings in combination with 3D printing encapsulation technology even in biomedical applications, specifically in the MRI environment.

The authors of this publication see the benefit in the FBG encapsulation detailed description of the method using the 3D printing method, which results in a sensor with very small dimensions of 10 × 5 × 2 mm and a weight of less than 5 g. Furthermore, the temperature and deformation characteristics of the sensor and results from long-term measurements of heart activity (heart rate) are described, including different ways to fix the sensor on the human body, all compared to a conventional ECG. The encapsulation process itself offers easy reproducibility and the sensor can be used repeatedly. Based on the measurements made, the sensor prototype represents an interesting alternative solution for the needs of sleep laboratories, magnetic resonance imaging environments, or environments in general where it is necessary to monitor cardiac activity over time.

II. METHODS

A. FIBER BRAGG GRATING (FBG)

The FBG is formed by a periodic change of refractive index in the core of an optical fiber. This periodic structure reflects a narrow part of the spectrum and transmits the rest of the spectrum without attenuation. The reflected wavelength is called the Bragg wavelength and is given by equation:

$$\lambda_B = 2\, n_{eff}\, \Lambda, \tag{1}$$

where n_{eff} is the effective refractive index of the grating structure and Λ is the period of refractive index changes. If temperature or strain acts on this structure, periodic changes occur, and the effective refractive index changes. This causes a shift of the reflected Bragg wavelength. The dependence of the Bragg wavelength on the applied temperature and strain is expressed by the following equation:

$$\frac{\Delta\lambda_B}{\lambda_B} = (1 - p_e)\,\varepsilon + (\alpha_n + \alpha_\Lambda)\,\Delta T, \tag{2}$$

where p_e is the photo-elastic coefficient, α_n is the temperature-optic coefficient and α_Λ is the thermal expansion coefficient. The temperature and strain coefficient vary with the absolute value of the Bragg wavelength. Therefore, a normalized strain coefficient at constant temperature is:

$$\frac{1}{\lambda_B}\frac{\Delta\lambda_B}{\Delta\varepsilon} = 0.78 \cdot 10^{-6}\mu\text{strain}^{-1} \tag{3}$$

and a normalized temperature coefficient at constant strain is:

$$\frac{1}{\lambda_B}\frac{\Delta\lambda_B}{\Delta T} = 6.678 \cdot 10^{-6\circ}C^{-1}. \tag{4}$$

B. BALLISTOCARDIOGRAPHY

Using the above-mentioned FBG sensor, the so-called ballistocardiograph signal (BCG) can be obtained. This method falls into the category of non-invasive sensing of body movements caused by the heart. Body movements measured by this method are caused by the acceleration of blood as it moves within large blood vessels [44]. Specifically, the consequence of blood impingement on the so-called aortic arch, which causes upward movement of the body and subsequent downward movement of the body as blood descends, is sensed. The current trend of using BCG type measurements is starting to increase again, thanks to new technologies, especially in the field of fiber-optic sensors; see Introduction. The progression or comparison of ECG and BCG is shown in Figure 1.

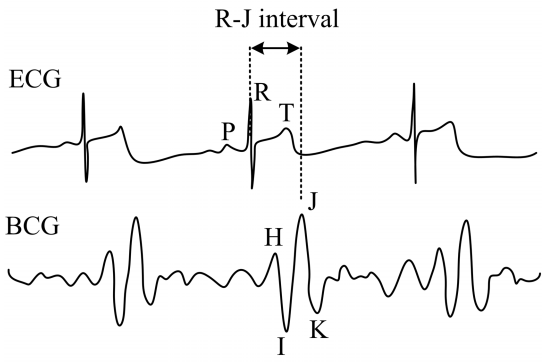

FIGURE 1. Course and comparison of ECG and BCG signals.

III. RESULTS

A. METHOD OF MEASURING HEART RATE WITH FBG

Due to the need to monitor cardiac activity, the position chosen for the experimental measurements was in the chest area, on the left side in the region of the heart (Figure 2 - marked in red). This position was chosen based on laboratory measurements primarily because it allows the contact area of the sensor with the human body, regardless of gender; see our previous publications where this issue was addressed [45].

To achieve the highest sensitivity of the measuring probe, it is necessary to choose a suitable method for implementation on the human body. In this section, the focus was on a flexible, easy, and comfortable way of implementation on the human body. For experimental measurements, two ways of implementing the measurement sensor were analyzed. These are implementation using a contact elastic strip (Figure 2(a)) or using a standard disposable hypoallergenic adhesive tape (Figure 2(b)), which is used for muscle and joint support and stability. The advantage of disposable hypoallergenic adhesive tape lies mainly in the very quick and easy implementation of the sensor on the human body.

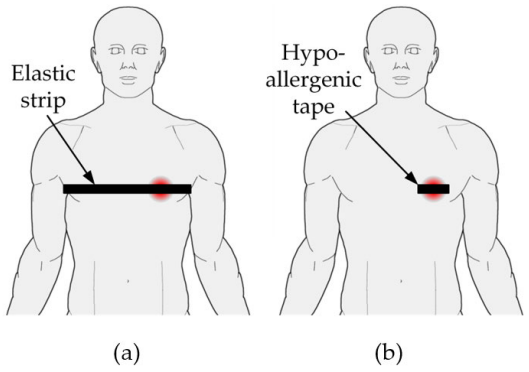

FIGURE 2. Placement of the measurement probe on the human body (shown in red) and how the sensor is implemented using an elastic strip (a) or hypoallergenic tape (b).

B. FBG SENSOR ENCAPSULATION INTO ACRYLONITRILE BUTADIENE STYRENE (ABS)

This section describes the complete process of encapsulating optical fiber with a Bragg grating into polymer layers during printing on a 3D printer. A large variety of materials can be used that differ in mechanical and thermal properties. ABS, which can withstand temperatures from −20 °C to 105 °C, was used to realize the prototype measurement probe. ABS exhibits a higher mechanical and lower temperature sensitivity compared to other commonly used materials such as PLA etc. Therefore, the ABS filament offers an optimal balance between strength and mechanical strain transfer while minimizing the effect of temperature fluctuations on the sensor output signal. These aspects are essential for this study because of the need to monitor very small vibrations caused by human heart activity and to reduce signal fluctuations due to changes in ambient temperature. The coefficient of thermal expansion of the ABS material ranges from $81 \cdot 10^{-6}$ to $95 \cdot 10^{-6} K^{-1}$, and the modulus of elasticity ranges from 2.0 GPa to 2.6 GPa. ABS is generally used for the manufacture of many products such as keyboard buttons, musical instrument components, medical devices, etc.

The prototype sensor consists of a 10×5×2 mm main sensing section and an end section for fixing and protecting the lead fiber. A standard apodized Bragg grating in acrylic protection with a central Bragg wavelength of 1557 nm, a reflectance spectral width of 230 pm and a reflectivity of 90 % was used to realize the sensor.

The process of manufacturing the prototype sensor was carried out in several steps. The Prusa i3 MK3S+ 3D printer (Prusa Research a.s., Prague, Czech republic) and ABS filament (Filament PM, Chudobin, Czech republic) with a diameter of 1.75 mm were used. First, the bottom part of the sensor was printed, which consisted of two layers with a thickness of 0.3 mm, and then the printing process was suspended. A bare optical fiber with a Bragg grating was placed on the bottom part so that the FBG in the primary protection was exactly in the middle of the sensor. The fiber was not glued to the bottom; it was only fixed with adhesive tape to the printing pad to prevent movement of the fiber when printing the sensor cover layer. This process was carried out very quickly to avoid significant cooling of the bottom layer material, which could have compromised the quality of the bond between the two layers.

This was followed by printing the top part of the sensor using two 0.3 mm thick layers. The thickness of the 0.3 mm layer was chosen with respect to the diameter of the filament in primary protection (250 μm) to prevent the filament from being torn off or deflected out of its central position when the nozzle passes over it. During printing, a 15% fill was chosen to achieve the necessary flexibility of the sensor itself. Subsequently, a 900 μm diameter protection tube was strung onto the optical fiber, followed by a shrink tube to ensure the protection tube was fixed to the sensor itself. The resulting sensor is shown in Figure 3(b).

C. THERMAL SENSITIVITY COEFFICIENT

The sensor temperature sensitivity was defined by measurements in a temperature box in a temperature range from -20 °C to 50 °C. The dependence of the Bragg wavelength

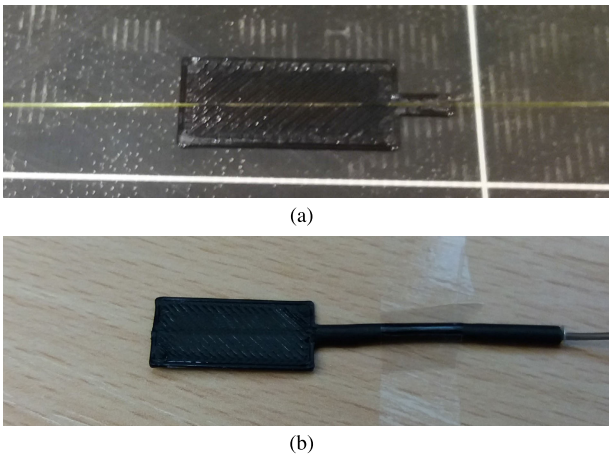

FIGURE 3. Encapsulation of the sensor: (a) placement of the optical fiber with a Bragg grating on the bottom layer; (b) the resulting FBG sensor.

on temperature is shown in Figure 4. A prototype sensor realized by encapsulating a Bragg grating with a wavelength of 1557 nm in ABS plastic shows a temperature sensitivity of 55.35 pm/°C, more than five times that of a bare Bragg grating according to normalized coefficient in equation 3 and in equation. 4. This temperature sensitivity was determined by a linear approximation of the measured data with a confidence value of R = 0.9518.

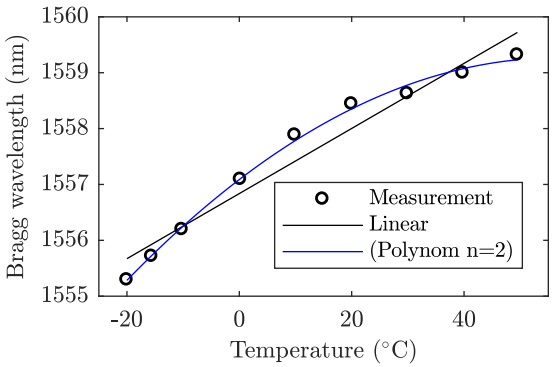

FIGURE 4. Temperature dependence of the Bragg wavelength of the prototype sensor with a marked linear and second-order polynomial approximation.

Due to the temperature-dependent coefficient of thermal expansion, the dependence of the Bragg wavelength of the measuring probe on temperature is a second-order polynomial function with a confidence value of R = 0.9968, so this dependence can be expressed by the following relation:

$$\lambda_B = -6.749 \cdot 10^{-4} T^2 + 0.07671 T + \lambda_{B0}, \tag{5}$$

where T is the applied temperature, λ_{B0} is the Bragg wavelength of the grating at room temperature and λ_B is the measured Bragg wavelength of the measuring probe at temperature T.

The determined average temperature sensitivity of the sensor is 55.35 pm/°C. This significant increase results from the differing thermal expansions of the materials (glass fiber, acrylic protection, ABS filament) and the adhesion between these materials, leading to an increase in the non-linearity of the temperature characteristic of the proposed sensor.

D. DEFORMATION SENSITIVITY COEFFICIENT

The strain sensitivity was determined by gluing a prototype sensor using cyanoacrylate adhesive to a 30 × 27.8 × 1 mm steel plate. This plate was placed in a hydraulic press in which it was loaded with a tensile force of 0 to 1910 N. The deformation of the steel plate is given by:

$$\varepsilon_{steel} = \frac{F}{SE}, \tag{6}$$

where F is the applied force, S is the cross section of the steel plate, and ε_{steel} is the modulus of elasticity of the steel with a value of 210 GPa. The deformation of the prototype sensor can be determined by the following relationship:

$$\varepsilon_{FBG} = \frac{\Delta\lambda_B}{k_\varepsilon}, \tag{7}$$

where $\Delta\lambda_B$ is the change in Bragg wavelength due to tensile loading and k_ε is the unknown deformation coefficient. This can be determined in two ways. First, equations 6 and 7 can be compared and the coefficient can be calculated according to the following relation:

$$k_\varepsilon = \frac{\Delta\lambda_{Bi} SE}{F_i}, \tag{8}$$

where $\Delta\lambda_{Bi}$ represents the measured change in the Bragg wavelength for a given value of F_i. The calculated coefficients for each measured force are given in Table 2. The second method is based on an optimization problem in which the minimum error is sought between the calculated steel strain ε_{steel} and the strain of the measuring probe ε_{FBG} in each of the n-measurements. The coefficient k_ε is then determined by solving the optimization problem by finding the minimum of the function $f\,(k_\varepsilon)$ on the interval $k \in \langle 1; 2\rangle$ according to the following relation:

$$f\,(k_\varepsilon) = Min \sum_{i=1}^{n} \left| \frac{F_i}{SE} - \frac{\Delta\lambda_{Bi}}{k_\varepsilon} \right|, \tag{9}$$

where F_i represents the set load and k_ε is the searched deformation sensitivity parameter. From the above analysis, also shown in Figure 5, the deformation coefficient was defined at 1.249 pm/μstrain.

The following table shows the values of the calculated mechanical stress and deformation of the steel plate, the measured deformation of the Bragg grating for different load values, and the calculated deformation coefficient at a given load step.

The Bragg wavelength shifts during steel plate loading with the applied forces listed in Table 2 are shown in

TABLE 2. Calculated and measured values of stress, steel deformation, and prototype sensor.

Force (N)	ε_{steel} (μstrain)	$\Delta\lambda_B$ (pm)	ε_{FBG} (μstrain)	ε_{error} (μstrain)	k_ε (pm/μstrain)
0.0	0.0	0.0	0.0	0.0	-
93.2	16.0	18.9	15.2	0.8	1.186
205.8	35.3	43.7	35.0	0.3	1.240
434.0	74.3	92.4	74.0	0.4	1.243
644.0	110.3	136.0	108.9	1.4	1.233
875.0	149.9	184.1	147.4	2.5	1.229
1070.0	183.3	228.9	183.3	0.0	1.249
1910.0	327.2	419.0	335.5	-8.3	1.281

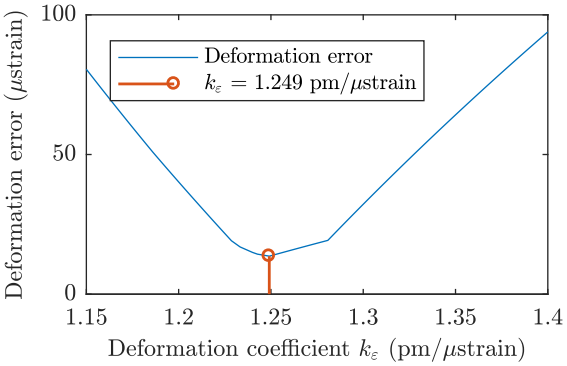

FIGURE 5. Determination of the deformation coefficient from the minimum error analysis.

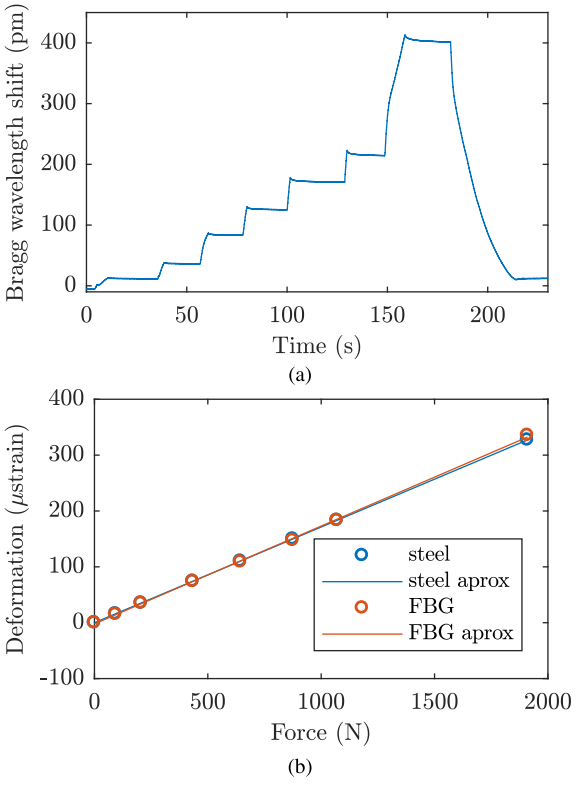

FIGURE 6. Dependence of the Bragg wavelength shift during loading of the steel plate (a); Dependence of the deformation of the steel and the Bragg grating on the applied force (b).

Figure 6(a). Figure 6(b) shows the dependence of the calculated steel strain and the measured Bragg grating strain on the applied force using a strain sensitivity factor of 1.249 pm/μstrain. The results show that the measuring probe with a Bragg grating encapsulated in ABS plastic exhibits a very good linear sensitivity to tensile stress.

E. SIGNAL PROCESSING

This chapter focuses on the analysis and interpretation of data obtained from Bragg grating-based sensors described in the previous chapters, describing the use of an interrogator unit to record the data, methods for filtering out noise, techniques for detecting peaks corresponding to heart rate, and procedures for smoothing the heart rate curve.

The FBGuard interrogator unit (Safibra s.r.o., Czech Republic), which uses the principle of spectral analysis of reflected light from Bragg gratings, was used to record data from the FBG sensors. Data recording was performed at a sampling rate of 1000 samples/s. The measurement scheme is shown in Figure 7(a).

Unwanted noise in the signal (muscle activity, motion artifacts) is created by higher frequencies, which are filtered out by a third-order digital Butterworth band-pass filter with cutoff frequencies of 1 and 15 Hz. Due to the lower cutoff frequency of 1 Hz, the fluctuation of the mean signal value caused by the varying depth of breathing of the test subjects over time is filtered out. The upper limit frequency was set at 15 Hz. At this cut-off frequency, sharpening of significant parts was ensured, which is important for the subsequent detection of beats during cardiac activity.

Subsequently, the signal is normalized and centered at zero mean. Peaks corresponding to heart rate (HR) are detected above this signal, from which the heart rate is calculated using the relation $HR = 60/(t_n - t_{n-1})$, where t_n is the time stamp of the n-th peak and t_{n-1} is the time stamp of the preceding peak. The following is the process of smoothing the heart rate curve. A median filter with a window size of 7 is used for smoothing, which is statistically more robust to outlying observations than the moving average; see Figure 7(b).

F. VERIFICATION OF SENSOR FUNCTIONALITY–HR MONITORING

Measurements were performed under laboratory conditions on 11 healthy test subjects with their written informed

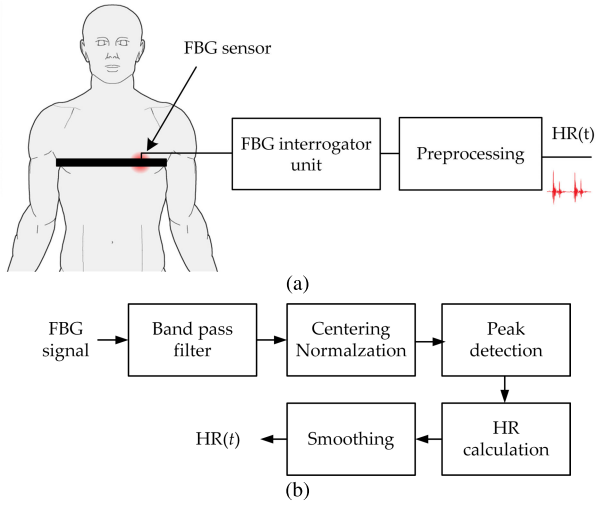

FIGURE 7. Basic schematic diagram of signal processing (a); Signal processing from the FBG sensor for HR determination (b).

consent. The test subjects were 6 male (M1 to M6) and 5 female (F1 to F5). The age of the test subjects ranged from 21 to 47 years, height from 154 to 189 cm, and weight from 48 to 96 kg. The test was performed in the supine body position to simulate the MRI and sleep laboratory environment. Each test subject was asked to simulate different breathing loads, i.e. deep and shallow breathing, during the measurements. A MIKROE-2455 3-lead ECG (Mikroe, Serbia) was used for the reference measurements.

1) SIGNAL WAVEFORMS DURING SIGNAL PROCESSING

In the following section, the waveforms of the measured signals and the influence of signal processing on these waveforms are shown for the selected subject M4.

Figure 8 shows ten-second examples of signals from FBG A (sensor fixed with an elastic strip) and FBG B (sensor fixed with adhesive tape).

For better readability of the sensor response to respiratory activity, the mean value is subtracted from the signal. At first glance, a sensor fixed with adhesive tape shows approximately 5 times greater response to human respiratory activity than a sensor fixed with an elastic band. Both fiber optic sensors record respiratory activity (breathing) and cardiac activity due to chest expansion. The signal corresponding to cardiac activity has a significantly smaller response and is modulated to the slow component of the signal corresponding to respiratory activity. Figure 9 shows the signal from the reference ECG device; in this case, no filtering is needed, only the R wave is detected.

To remove the DC component and filter out the slow components in FBG sensors that correspond to respiratory activity, a third-order Butterworth bandpass filter with cutoff frequencies of 1 and 15 Hz is applied to the measured signals. The filtered signal from FBG A is shown in Figure 10(a), and the filtered signal from FBG B is shown in Figure 10(b). For both, the detected peaks corresponding to cardiac activity are

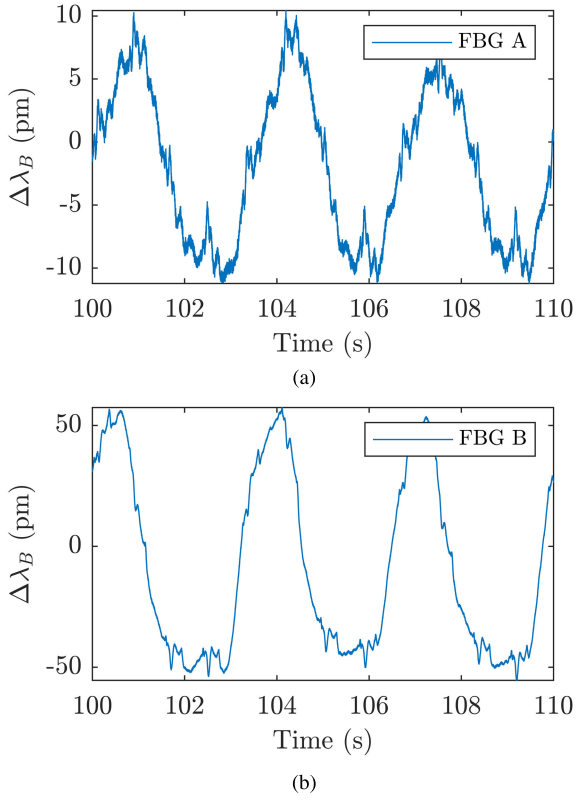

FIGURE 8. Detail of the signal measured from the sensors (a) FBG A fixed with elastic strip and (b) FBG B fixed with adhesive tape.

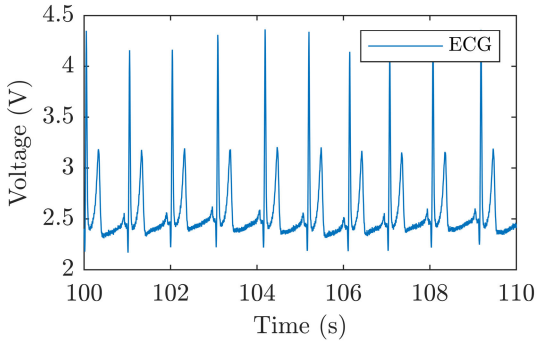

FIGURE 9. Signal from the reference ECG.

marked. Peak detection in the signal was carried out in the MATLAB environment using the findpeaks function, with the MinPeakProminence and MinPeakDistance carefully adjusted for each subject tested to achieve the most accurate estimate of cardiac activity.

Figure 11 shows a comparison of the 10-second signals from FBG sensor A fixed with an elastic band and the ECG signal. It can be seen from the figure that the detection of cardiac activity by the FBG sensor is fully correlated with the reference ECG signal. The waveforms also show a lower signal-to-noise ratio for the FBG sensor, which is due to the bandpass filtering of the signals (1 to 15 Hz) and thus the reduced bandwidth of the FBG sensor. However, the results described in the next section demonstrate that the FBG

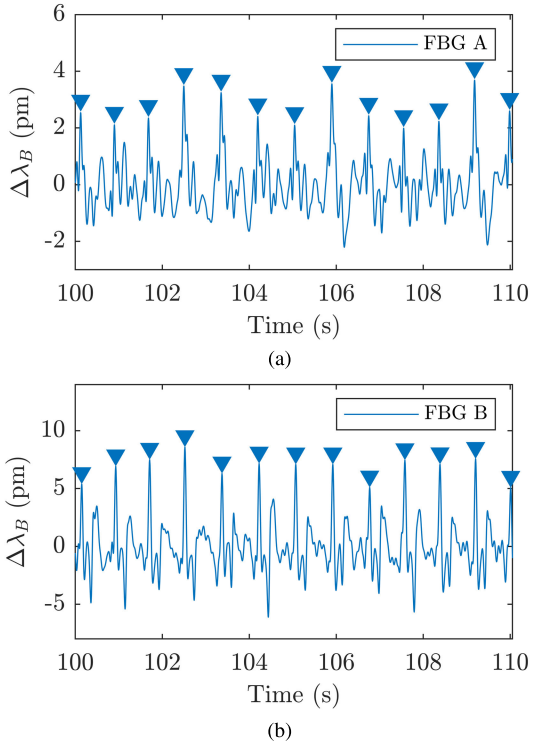

FIGURE 10. Detail of the signal measured from the sensors (a) FBG A fixed with elastic strip and (b) FBG B fixed with adhesive tape.

sensor is suitable as an alternative method to monitor cardiac activity.

The filtered signal from the FBG has a significantly smaller signal-to-noise ratio and also a smaller bandwidth due to filtering compared to the signal from the reference ECG. However, even in this way individual heartbeats are well detected, as shown in Figure 11.

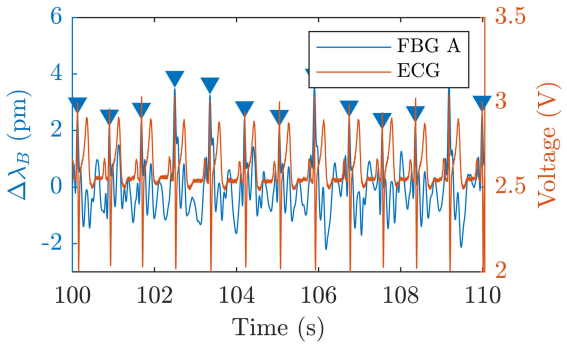

FIGURE 11. Comparison of waveforms of the FBG sensor A fixed with an elastic band and the reference ECG signal.

From the time stamps of each peak, the heart rate is calculated using the formula $HR_i = 60/(t_i - t_{i-1})$, where HR_i corresponds to the heart rate, t_i is the timestamp of the i-th peak and $t_{i-1)}$ is the timestamp of the preceding peak. The calculated heart rate values for both sensors are compared with the calculated heart rate from the reference

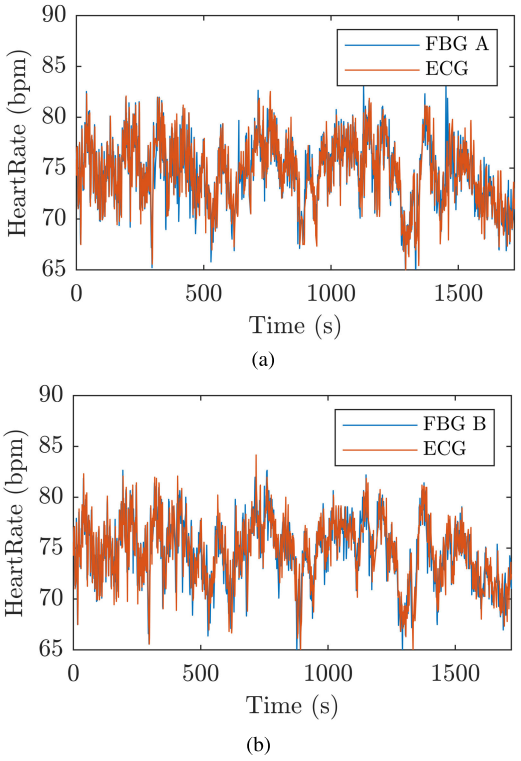

FIGURE 12. Comparison of HR from the fiber optic sensor and the reference ECG for (a) FBG A and (b) FBG B.

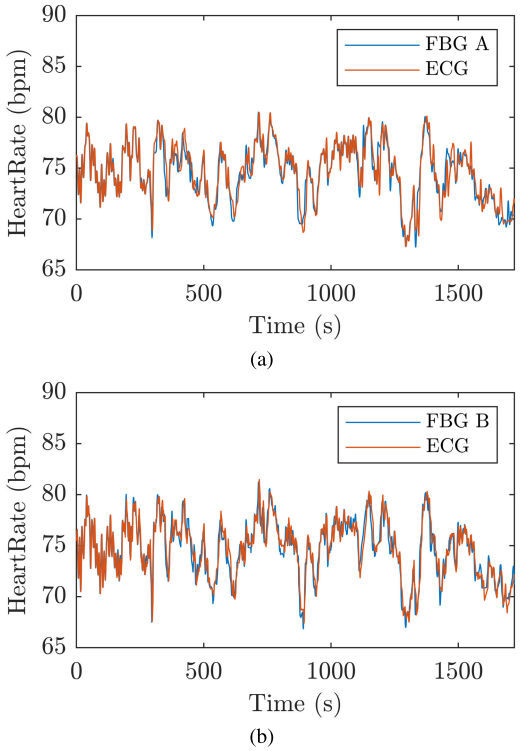

FIGURE 13. Smoothed HR waveforms using median filter for (a) FBG A and (b) FBG B.

ECG sensor and shown in Figure 12(a) for the FBG A sensor and Figure 12(b) for the FBG B sensor.

TABLE 3. HR errors for individual subjects and sensors.

	N (-)			Mean HR (bpm)			σ^2 (bpm)		E (bpm)		EI (bpm)	
	A	B	ECG	A	B	ECG	A	B	A	B	A	B
M1	2235	2229	2236	74.65	74.67	74.69	7.63	10.32	0.10	-0.08	±5.98	±5.98
M2	1711	1737	1739	60.61	56.34	59.17	9.80	9.66	-0.05	-0.08	±5.99	±5.98
M3	1528	1553	1554	52.91	52.01	51.16	4.06	9.96	0.01	0.47	±3.99	±5.97
M4	2154	2268	2269	72.14	72.31	72.26	6.54	1.99	0.08	-0.01	±4.97	±2.99
M5	1398	1417	1425	56.65	53.77	55.31	2.38	6.23	0.03	0.19	±2.97	±4.99
M6	2107	2121	2121	74.72	74.71	74.76	3.88	3.65	-0.04	0.07	±4.97	±3.99
F1	2127	2128	2157	53.97	57.67	53.06	9.05	7.79	0.01	0.14	±5.99	±5.95
F2	1510	1515	1575	75.23	75.89	75.35	11.68	6.71	-0.19	-0.02	±6.98	±4.99
F3	2106	2221	2227	62.23	62.00	62.15	16.93	6.58	0.41	-0.05	±7.94	±4.99
F4	1857	1848	1879	70.84	71.33	71.09	6.92	19.34	0.00	0.01	±4.99	±9.99
F5	1906	1901	1908	65.69	64.03	64.51	5.18	5.16	-0.26	-0.14	±3.99	±3.99
Mean values							7.64	7.94	0.10	0.11	±5.34	±5.44

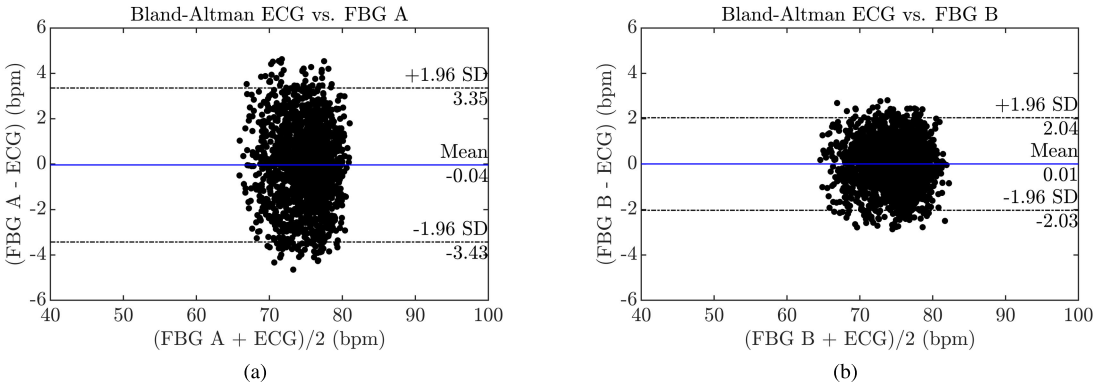

FIGURE 14. Bland-Altman plot of the sensor success rate in HR measurement of subject M6 using (a) FBG A and (b) FBG B.

To eliminate noise, the signal was further smoothed using a median average with a window size of 7 samples; see Figure 13. All measured data were processed in a similar manner and subjected to further analysis, which is described in the following section.

2) SENSOR COMPARISON IN THE TIME DOMAIN

Based on the processing of the filtered signals and the HR calculation, the analysis of the results was performed and is summarized in Table 3. For each subject and sensor, the number of detected peaks N and the subsequently calculated heart rate variance σ^2 according to equation 10 are given:

$$\sigma^2 = \frac{1}{N}\sum_{i=1}^{N}\left(HR_{FBG,i} - HR_{ECG,i}\right)^2, \tag{10}$$

where $HR_{FBG,n}$ is the n-th HR value calculated from the FBG fiber optic sensor and $HR_{ECG,n}$ je n-th HR value calculated from the reference ECG device. The table also shows the average value of the heart rate error E calculated according to equation 11:

$$E = \frac{1}{N}\sum_{i=1}^{N} HR_{FBG,i} - HR_{ECG,i}, \tag{11}$$

and the interval of these errors according to equation 12.

$$EI = max\left(HR_{FBG} - HR_{ECG}\right) - min\left(HR_{FBG} - HR_{ECG}\right). \tag{12}$$

3) COMPARISON OF SENSORS USING BLAND-ALTMAN ANALYSIS

For two selected subjects, Figures 14 and 15 show B-A plots that graphically represent the sensor success rate compared to a reference ECG sensor. In Figure 14, the B-A analysis of the selected male subject M6 is shown, where 92.28% of all samples lie within ±1.96 SD (Standard Deviation) for the FBG A sensor, see Figure 14(a) and 95.9% for the FBG B sensor, see Figure 14(b). Similarly, the Bland-Altman analysis for the female subject F2 is depicted graphically; in the case of FBG A, 95.11% of all samples lie within ±1.96 SD, see Figure 15(a), while in the case of FBG B, a total of 95.15% of samples lie within ±1.96 SD, see Figure 15(b).

A statistical summary of the collected data is shown in Table 4. The first column represents the subject designation, and the second column indicates the type of Bragg sensor (FBG A sensor fixed with elastic strip, FBG B sensors fixed with adhesive tape). The other columns are related to the Bland-Altman (B-A) statistic. MoD represents the

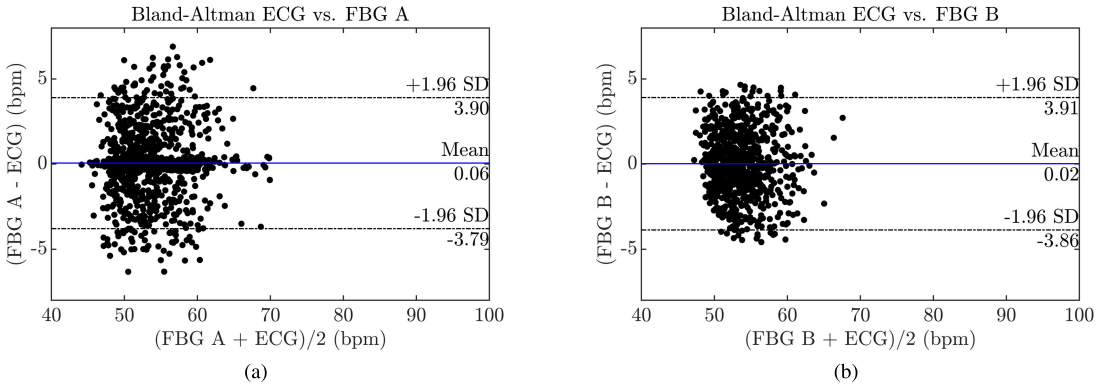

FIGURE 15. Bland-Altman plot of the sensor success rate in HR measurement of subject F2 using (a) FBG A and (b) FBG B.

TABLE 4. Statistical summary of the data collected.

Subject	Sensor FBG	MoD (bpm)	SD pos (bpm)	SD neg (bpm)	±1.96 SD (bpm)	Error (bpm)	Success rates (%)
M1	A	-0.10	3.96	-4.16	8.15	86	95.44
	B	0.09	3.72	-3.55	7.27	54	96.06
M2	A	0.05	4.58	-4.48	9.06	31	95.07
	B	0.07	4.63	-4.48	9.11	58	95.06
M3	A	-0.01	2.73	-2.75	5.47	60	95.25
	B	-0.47	2.83	-3.77	6.60	45	95.28
M4	A	-0.08	3.94	-4.09	8.04	31	97.92
	B	0.01	2.04	-2.03	4.07	104	94.59
M5	A	-0.03	2.17	-2.23	4.40	38	95.81
	B	-0.19	3.34	-3.72	7.05	40	95.37
M6	A	0.04	3.07	-2.99	6.06	110	92.28
	B	-0.07	2.70	-2.85	5.55	63	95.90
F1	A	-0.10	3.48	-3.67	7.15	67	95.46
	B	-0.14	3.95	-4.24	8.19	48	95.80
F2	A	0.19	5.26	-4.88	10.14	55	95.11
	B	0.02	3.68	-3.64	7.32	46	95.15
F3	A	-0.41	3.77	-4.59	8.36	23	96.74
	B	0.05	3.16	-3.07	6.23	60	95.18
F4	A	0.00	4.19	-4.19	8.39	33	97.44
	B	-0.01	4.57	-4.59	9.16	81	95.27
F5	A	0.26	3.46	-3.95	7.41	44	95.93
	B	0.14	3.27	-2.98	6.25	28	95.67
Mean values	A	0.12	3.69	-3.82	7.51	53	95.68
	B	0.11	3.44	-3.54	6.98	57	95.39

mean value of the difference between the FBG and the reference sensor, SD pos (Standard Deviation positive) and SD neg (Standard Deviation negative) represent the interval ±1.96 SD (Standard Deviation), respectively. The error column shows the number of samples that lie outside the ±1.96 SD interval, and the last column, Success rates, shows the percentage of samples that lie within the calculated ±1.96 SD interval.

Based on these results (Table 3 and Table 4), it is not possible to clearly identify a sensor that performs better in terms of measurement variance or error rate. However, it is clear from the error results that the range is relatively small, within 6% for males and within 10% for female test subjects. Furthermore, due to the lower signal response of sensor A, a lower number of heartbeats are detected compared to sensor B or the reference ECG. However, sensor A achieved on average a slightly higher success rate (95.68% vs. 95.39% for sensor B). Considering that for both sensors over 95% of the values were within ±1.96 SD interval and the MoD values were close to 0, it can be said that there is no statistically significant difference between the ECG and FBG methods.

IV. CONCLUSION

This article provides new insights and a comprehensive description of the possibility of encapsulating fiber Bragg grating (FBG) using 3D printing technology. One of the possible applications and use cases of such a realized sensor is in biomedicine, especially in the field of magnetic resonance (MR) or sleep laboratory, where the complete EMI resistance, small size of fiber optic cables, and low sensor weight are great advantages. The material chosen for the FBG encapsulation was acrylonitrile butadiene styrene (ABS). The actual implementation of FBG encapsulation was divided into several steps, which are described in detail in the article,

including a description of the temperature and strain sensitivity coefficients. For validation in terms of applicability in biomedicine, a long-term experimental investigation of heart rate (HR) measurements was performed on 11 volunteers of different gender and body measures against a standard Electrocardiography (ECG). We have obtained excellent results based on the objective Bland-Altman method (B-A) that a reliability of HR monitoring is over 95%.

V. DISCUSSION

This study represents an initial step in the use of ABS material for Bragg grating encapsulation with the aim of obtaining a prototype sensor suitable for use in heart rate monitoring. ABS material was chosen primarily for its combination of properties suitable for encapsulating fiber Bragg gratings. For this reason, the authors' team focused in particular on a detailed description of the different stages of the Bragg grating encapsulation process, including an analysis of the temperature and strain dependence, which we believe will provide original and interesting findings for the scientific community.

Furthermore, in order to meet the need for use in biomedical applications and in real world practice, it is important to achieve a solution that is minimal in terms of weight and size but exhibits a high level of reliability and accuracy. These aspects have been a downstream motivation for the author team, resulting in a sensor defined by compact dimensions of 10 × 5 × 2 mm and a weight of <5g. Practical validation was carried out in a study of 11 volunteers with an average error of 0.10 bpm for sensor A and 0.11 bpm for sensor B and success rates based on the Bland Altman of 95.68% and 95.38% for sensor A and sensor B, respectively. A key motivation of the author's team was also to select a material type that would maintain the original electromagnetic compatibility. This is one of the main benefits of fiber optic technology, especially for use in electromagnetically interfered environments such as MRI. In these environments, conventional technologies such as ECGs based on the measurement of electrical potentials show a reduction in functional reliability, and it is therefore necessary to look for solutions that can be complementary to these conventional sensors in the near future.

The next step of this study will be to validate and test the sensor in a real MRI environment in cooperation with our partner CEITEC MU Brno (Czech Republic) in various test sequences and to demonstrate the suitability of the combination of ABS and FBG material for the measurement of vital functions of the human body in MR including MR synchronization (triggering). In particular, MR synchronization by innovative types of sensors is a very topical issue, and there is a large space for scientific research. In medical terms, we are talking about patients where the ability of patient-doctor cooperation is reduced, i.e., elderly people and children under 5 years of age. Here, we see one of the main potential benefits of the presented sensory solution.

REFERENCES

[1] M. Zabel, B. Acar, T. Klingenheben, M. R. Franz, S. H. Hohnloser, and M. Malik, "Analysis of 12-lead T-Wave morphology for risk stratification after myocardial infarction," *Circulation*, vol. 102, no. 11, pp. 1252–1257, Sep. 2000.

[2] R. Ogura, Y. Hiasa, T. Takahashi, K. Yamaguchi, K. Fujiwara, Y. Ohara, T. Nada, T. Ogata, K. Kusunoki, K. Yuba, S. Hosokawa, K. Kishi, and R. Ohtani, "Specific findings of the standard 12-lead ECG in patients with 'Takotsubo' cardiomyopathy-comparison with the findings of acute anterior myocardial infarction-: Comparison with the findings of acute anterior myocardial infarction," *Circulat. J.*, vol. 67, no. 8, pp. 687–690, 2003.

[3] M. S. Nacif, A. Zavodni, N. Kawel, E.-Y. Choi, J. A. C. Lima, and D. A. Bluemke, "Cardiac magnetic resonance imaging and its electrocardiographs (ECG): Tips and tricks," *Int. J. Cardiovascular Imag.*, vol. 28, no. 6, pp. 1465–1475, Oct. 2011.

[4] D. Abi-Abdallah, V. Robin, A. Drochon, and O. Fokapu, "Alterations in human ECG due to the MagnetoHydroDynamic effect: A method for accurate R peak detection in the presence of high MHD artifacts," in *Proc. 29th Annu. Int. Conf. IEEE Eng. Med. Biol. Soc.* IEEE, Aug. 2007, pp. 1842–1845.

[5] W. Wang, S. Weiss, A. C. den Brinker, J. H. Wuelbern, A. G. I. Tormo, I. Pappous, and J. Sénégas, "Fundamentals of camera-PPG based magnetic resonance imaging," *IEEE J. Biomed. Health Informat.*, vol. 26, no. 9, pp. 4378–4389, Sep. 2022.

[6] R. Martinek, J. Brablik, J. Kolarik, M. Ladrova, J. Nedoma, R. Jaros, L. Soustek, R. Kahankova, M. Fajkus, L. Vojtisek, P. Hanzlikova, and P. Krupa, "A low-cost system for seismocardiography-based cardiac triggering: A practical solution for cardiovascular magnetic resonance imaging at 3 Tesla," *IEEE Access*, vol. 7, pp. 118608–118629, 2019.

[7] M. Weckesser, S. Posse, U. Olthoff, L. Kemna, S. Dager, and H.-W. Müller-Gärtner, "Functional imaging of the visual cortex with bold-contrast MRI: Hyperventilation decreases signal response," *Magn. Reson. Med.*, vol. 41, no. 1, pp. 213–216, Jan. 1999.

[8] Z. Chen, H. I. Hee, S. H. Ng, J. T. Teo, X. Yang, and D. Wang, "Microbend fiber optic sensor for perioperative pediatric vital signs monitoring," in *Optical Fibers and Sensors for Medical Diagnostics and Treatment Applications XVII*, vol. 10058, I. Gannot, Ed. Bellingham, WA, USA: SPIE, 2017, pp. 100580L1–100580L8.

[9] I. Sadek, E. Seet, J. Biswas, B. Abdulrazak, and M. Mokhtari, "Nonintrusive vital signs monitoring for sleep apnea patients: A preliminary study," *IEEE Access*, vol. 6, pp. 2506–2514, 2018.

[10] T. Sirkis, Y. Beiderman, S. Agdarov, Y. Beiderman, and Z. Zalevsky, "Fiber sensor for non-contact estimation of vital bio-signs," *Opt. Commun.*, vol. 391, pp. 63–67, May 2017.

[11] F. Xie, J. Ren, Z. Chen, and Q. Feng, "Vibration-displacement measurements with a highly stabilised optical fiber Michelson interferometer system," *Opt. Laser Technol.*, vol. 42, no. 1, pp. 208–213, Feb. 2010.

[12] T. Kumagai and S. Sato, "Development of Sagnac interferometer-type optical fiber vibration sensor for physical security," *IEEJ Trans. Sensors Micromachines*, vol. 132, no. 11, pp. 407–412, 2012.

[13] S. Wu, L. Wang, X. Chen, and B. Zhou, "Flexible optical fiber Fabry–Perot interferometer based acoustic and mechanical vibration sensor," *J. Lightw. Technol.*, vol. 36, no. 11, pp. 2216–2221, Jun. 1, 2018.

[14] D. Zazula, D. Đonlagić, and S. Šprager, "Application of fibre-optic interferometry to detection of human vital signs," *J. Laser Health Acad.*, vol. 2012, no. 1, pp. 27–32, 2012.

[15] C. Campanella, A. Cuccovillo, C. Campanella, A. Yurt, and V. Passaro, "Fibre Bragg grating based strain sensors: Review of technology and applications," *Sensors*, vol. 18, no. 9, p. 3115, Sep. 2018.

[16] C. P. Mayoral, J. G. Gutiérrez, J. L. C. Pérez, M. V. Treviño, I. B. G. Velasco, P. A. H. Cruz, R. T. Rosas, L. T. Carrillo, J. Arnaud Ríos, E. L. Apreza, and R. R. Laguna, "Fiber optic sensors for vital signs monitoring. A review of its practicality in the health field," *Biosensors*, vol. 11, no. 2, p. 58, Feb. 2021.

[17] L. Dziuda, M. Krej, and F. W. Skibniewski, "Fiber Bragg grating strain sensor incorporated to monitor patient vital signs during MRI," *IEEE Sensors J.*, vol. 13, no. 12, pp. 4986–4991, Dec. 2013.

[18] J. Hao, M. Jayachandran, P. L. Kng, S. F. Foo, P. W. A. Aung, and Z. Cai, "FBG-based smart bed system for healthcare applications," *Frontiers Optoelectronics China*, vol. 3, no. 1, pp. 78–83, Jan. 2010.

[19] C. Massaroni, M. Zaltieri, D. Lo Presti, A. Nicolò, D. Tosi, and E. Schena, "Fiber Bragg grating sensors for cardiorespiratory monitoring: A review," *IEEE Sensors J.*, vol. 21, no. 13, pp. 14069–14080, Jul. 2021.

[20] R. Rohan, K. Venkadeshwaran, and P. Ranjan, "Recent advancements of fiber Bragg grating sensors in biomedical application: A review," *J. Opt.*, vol. 53, no. 1, pp. 282–293, Feb. 2024.
[21] J. Nedoma, M. Fajkus, P. Siska, R. Martinek, and V. Vasinek, "Non-invasive fiber optic probe encapsulated into PolyDiMethylSiloxane for measuring respiratory and heart rate of the human body," *Adv. Elect. Electron. Eng.*, vol. 15, no. 1, pp. 93–100, Mar. 2017.
[22] M. Fajkus, J. Nedoma, R. Martinek, V. Vasinek, H. Nazeran, and P. Siska, "A non-invasive multichannel hybrid fiber-optic sensor system for vital sign monitoring," *Sensors*, vol. 17, no. 12, p. 111, Jan. 2017.
[23] D. Lo Presti, D. Bianchi, C. Massaroni, A. Gizzi, and E. Schena, "A soft and skin-interfaced smart patch based on fiber optics for cardiorespiratory monitoring," *Biosensors*, vol. 12, no. 6, p. 363, May 2022.
[24] W. B. SpillmanJr, M. Mayer, J. Bennett, J. Gong, K. E. Meissner, B. Davis, R. O. Claus, A. A. MuelenaerJr, and X. Xu, "A smart bed for non-intrusive monitoring of patient physiological factors," *Meas. Sci. Technol.*, vol. 15, no. 8, pp. 1614–1620, Jul. 2004.
[25] M. Ciocchetti, C. Massaroni, P. Saccomandi, M. Caponero, A. Polimadei, D. Formica, and E. Schena, "Smart textile based on fiber Bragg grating sensors for respiratory monitoring: Design and preliminary trials," *Biosensors*, vol. 5, no. 3, pp. 602–615, Sep. 2015.
[26] K.-L. Wong, C.-C. Chiang, and S.-H. Wang, "A novel radio frequency identification (RFID)-based thermal convection nonfloating-type accelerometer with stacking layers under heater and thermal sensors," *Sensors Mater.*, vol. 27, no. 8, pp. 651–662, Sep. 2015.
[27] P. C. Liacouras, G. T. Grant, K. Choudhry, G. F. Strouse, and Z. Ahmed, "Fiber Bragg gratings embedded in 3D-printed scaffolds," *NCSLI Measure*, vol. 10, no. 2, pp. 50–52, Jun. 2015.
[28] M. G. Zubel, K. Sugden, D. Saez-Rodriguez, K. Nielsen, and O. Bang, "3D printed sensing patches with embedded polymer optical fibre Bragg gratings," in *Proc. 6th Eur. Workshop Opt. Fibre Sensors*, vol. 9916, E. Lewis, Ed. Bellingham, WA, USA: SPIE, 2016, Art. no. 99162E.
[29] A. G. Leal-Junior, C. Marques, M. R. N. Ribeiro, M. J. Pontes, and A. Frizera, "FBG-embedded 3-D printed ABS sensing pads: The impact of infill density on sensitivity and dynamic range in force sensors," *IEEE Sensors J.*, vol. 18, no. 20, pp. 8381–8388, Oct. 2018.
[30] A. Lacraz, M. Zubel, G. Demirci, A. Theodosiou, K. Kalli, K. Sugden, and B. Gawdzik, "Embedding low loss polymer optical fibre Bragg gratings: Two different approaches," in *Proc. 25th Int. Conf. Plastic Opt. Fibres*, U.K., Sep. 2016, pp. 36–39.
[31] H. Ahmad, M. A. Alias, M. F. Ismail, N. N. Ismail, M. K. A. Zaini, K. S. Lim, G. Brambilla, K. T. V. Grattan, and B. M. A. Rahman, "Strain sensor based on embedded fiber Bragg grating in thermoplastic polyurethane using the 3D printing technology for improved sensitivity," *Photon. Sensors*, vol. 12, no. 3, pp. 1–11, Jan. 2022.
[32] R. Zelený and J. Včelák, "Strain measuring 3D printed structure with embedded fibre Bragg grating," *Proc. Eng.*, vol. 168, pp. 1338–1341, 2016.
[33] L. Fang, T. Chen, R. Li, and S. Liu, "Application of embedded fiber Bragg grating (FBG) sensors in monitoring health to 3D printing structures," *IEEE Sensors J.*, vol. 16, no. 17, pp. 6604–6610, Sep. 2016.
[34] D. Paloschi, A. Polimadei, S. Korganbayev, V. Orsetti, A. Cigada, M. Caponero, and P. Saccomandi, "Fiber Bragg gratings embedded inside 3d-printed patches—Sensor design and mechanical characterization," in *Proc. IEEE Int. Workshop Metrol. Living Environ. (MetroLivEnv)*. IEEE, May 2023, pp. 45–49.
[35] D. Paloschi, A. Polimadei, S. Korganbayev, V. Orsetti, C. Mazzotta, A. Cigada, M. A. Caponero, and P. Saccomandi, "Three-dimensional-printed sensing samples embedding fiber Bragg gratings: Metrological evaluation of different sample materials and fiber coatings," *IEEE Trans. Instrum. Meas.*, vol. 72, pp. 1–10, 2023.
[36] N. N. Ismail, A. S. Sharbirin, M. S. M. Sa'ad, M. K. A. Zaini, M. F. Ismail, G. Brambilla, B. M. A. Rahman, K. T. V. Grattan, and H. Ahmad, "Novel 3D-printed biaxial tilt sensor based on fiber Bragg grating sensing approach," *Sens. Actuators A, Phys.*, vol. 330, Oct. 2021, Art. no. 112864.
[37] Z. Wang, M. Liu, Y. Qu, Q. Wei, Z. Zhou, Y. Tan, L. Hong, and J. Zhang, "An FBG based smart clamp fabricated by 3D printing technology and its application to incipient clamp looseness detection," in *Proc. IEEE Int. Conf. Prognostics Health Manage. (ICPHM)*, Jun. 2019, pp. 1–10.
[38] C. Tavares, C. Leitão, D. Lo Presti, M. F. Domingues, N. Alberto, H. Silva, and P. Antunes, "Respiratory and heart rate monitoring using an FBG 3D-printed wearable system," *Biomed. Opt. Exp.*, vol. 13, no. 4, p. 2299, Mar. 2022.
[39] C. Tavares, C. Leitão, D. Lo Presti, E. Schena, M. F. Domingues, N. Alberto, H. P. Da Silva, and P. Antunes, "3D printed wearable FBG based devices: A proof of concept for heart rate monitoring," in *Proc. IEEE Int. Workshop Metrology Ind. 4.0 IoT (MetroInd4.0&IoT)*, Jun. 2022, pp. 366–370.
[40] M. Kostelanský, M. Fridrich, and J. Jargus, "FBG sensor encapsulated by using 3D printing technology for monitoring the heart rate of the human body," in *Emerging Imaging and Sensing Technologies for Security and Defence VII*, vol. 12274, G. S. Buller, R. C. Hollins, R. A. Lamb, and M. Laurenzis, Eds. Bellingham, WA, USA: SPIE, 2022, Art. no. 122741C.
[41] A. C. Nepomuceno, N. Alberto, P. André, P. F. D. C. Antunes, and M. D. F. Domingues, "3D printed spirometer for pulmonary health assessment based on fiber Bragg gratings," *IEEE Sensors J.*, vol. 21, no. 4, pp. 4590–4598, Feb. 2021.
[42] J. Nedoma, M. Kostelansky, D. Vilimek, M. Ladrova, R. Martinek, R. Kahankova, M. Fajkus, J. Brablik, P. Hanzlikova, M. A. Mohammed, and K. Behbehani, "Fiber-optic breathing mask: An alternative solution for MRI respiratory triggering," *IEEE Trans. Instrum. Meas.*, vol. 71, pp. 1–13, 2022.
[43] F. De Tommasi, C. Massaroni, M. A. Caponero, E. Schena, D. L. Presti, and M. Carassiti, "Wearable 3D-printed thumb-shaped device based on fiber Bragg grating sensor for epidural space detection," *IEEE Sensors J.*, vol. 23, no. 15, pp. 16907–16914, Aug. 2023.
[44] E. Pinheiro, O. Postolache, and P. Girão, "Theory and developments in an unobtrusive cardiovascular system representation: Ballistocardiography," *Open Biomed. Eng. J.*, vol. 4, no. 1, pp. 201–216, Oct. 2010.
[45] J. Nedoma, R. Martinek, M. Fajkus, J. Brablik, R. Kahankova, M. Fridrich, M. Kostelansky, P. Hanzlikova, L. Vojtisek, and K. Behbehani, "A novel FBG-based triggering system for cardiac MR imaging at 3 Tesla: A pilot pre-clinical study," *IEEE Access*, vol. 8, pp. 181205–181223, 2020.

M. FAJKUS was born in Czech Republic, in 1987. In 2017, he successfully defended his dissertation thesis and works as an Assistant Professor with the VSB—Technical University of Ostrava. He has more than 144 journals and conference papers and seven valid patents. His current research interests include fiber Bragg sensors and distributed systems in traffic, civil engineering, and biomedical applications.

M. KOSTELANSKY was born in Hodonin, Czech Republic, in 1993. He received the bachelor's and master's degrees in information technologies from the Department of Information and Communications Technologies, Faculty of Electrical Engineering and Computer Science, VSB—Technical University of Ostrava, in 2016 and 2019, respectively, where he is currently pursuing the Ph.D. degree. His current research interests include fiber-optic sensors predominantly in biomedical applications, traffic, and civil engineering.

M. FRIDRICH was born in Trutnov, Czech Republic, in 1995. He received the bachelor's and master's degrees in information and communication technology from the VSB—Technical University of Ostrava, in 2017 and 2019, where he is currently pursuing the Ph.D. degree, with a focus on fiber Bragg sensors and distributed systems in transportation, construction, and biomedical applications.

J. CUBIK was born in Olomouc, in 1986. He received the bachelor's and master's degrees in telecommunications from the Faculty of Electrical Engineering and Computer Science, Department of Telecommunications, VSB—Technical University of Ostrava, Ostrava, Czech Republic, in 2009 and 2011, respectively. In 2018, he successfully defended his dissertation thesis with the VSB—Technical University of Ostrava. He is currently an Assistant Professor for science and research and he works in the field of optical communications and fiber optic sensor systems.

S. KEPAK was born in Ostrava, Czech Republic, in 1987. He received the master's degree in telecommunications and the Ph.D. degree in communication technology from the VSB–Technical University of Ostrava, Ostrava, in 2011 and 2018, respectively. He has been with the VSB–Technical University of Ostrava, since 2013. He has authored/coauthored more than 50 articles and three inventions. His research interests include fiber optic sensors, especially fiber optic interferometers.

D. KRIZAN was born in Havířov, in 1996. He received the bachelor's and master's degrees from the Faculty of Electrical Engineering and Informatics, VSB—Technical University of Ostrava, in 2020, where he is currently pursuing the Ph.D. degree. In these studies, he specializes in fiber optic sensors, fiber Bragg sensors, and its application in biomedicine.

R. MARTINEK (Senior Member, IEEE) was born in Czech Republic, in 1984. He received the master's degree in information and communication technology from the VSB—Technical University of Ostrava, in 2009. Since 2012, he has been a Research Fellow. In 2014, he successfully defended his dissertation thesis titled "The Use of Complex Adaptive Methods of Signal Processing for Refining the Diagnostic Quality of the Abdominal Fetal Electrocardiogram." He was an Associate Professor of technical cybernetics, in 2017, after defending the habilitation thesis titled "Design and Optimization of Adaptive Systems for Applications of Technical Cybernetics and Biomedical Engineering Based on Virtual Instrumentation." He has been an Associate Professor with the VSB—Technical University of Ostrava, since 2017. His current research interests include digital signal processing (linear and adaptive filtering, soft computing—artificial intelligence and adaptive fuzzy systems, non-adaptive methods, biological signal processing, and digital processing of speech signals), wireless communications (software-defined radio), and power quality improvement. He has more than 200 journals and conference papers in his research areas.

MAZIN ABED MOHAMMED received the B.Sc. degree in computer science from the College of Computer, University of Anbar, Ramadi, Iraq, the master's degree in IT from Universiti Tenaga Nasional Malaysia, and the Ph.D. degree in biomedical computing and AI from Universiti Teknikal Malaysia Melaka, Malaysia. He is currently an Associate Professor with the Department of Information Systems, College of Computer Science and Information Technology, University of Anbar. His outstanding scientific production spans more than 110 contributions published in high-standard ISI journals, such as IEEE Internet of Things Journal, IEEE Transactions on Intelligent Transportation Systems, *Journal of King Saud University Computer and Information Sciences*, IEEE Access, *Future Generation Computer Systems*, *International Journal of Medical Informatics*, *Computers and Electrical Engineering*, *Journal of Computational Science*, and *Journal of Medical Systems*. He has published more than 210 papers in international journals and conferences and total number of citations over 3446 (Google Scholar H-Index = 51). He has collaborated with over 25 international countries and more than 150 researchers. His current research interests include artificial intelligence, data science, medical image processing, computer vision, computational intelligence, the IoT, biomedical computing, bio-informatics, big data analytics, the IoT applications, and fog Computing. He has served as an editor, an associate editor, a guest editor, and a reviewer for more than 100 international journals.

J. NEDOMA (Senior Member, IEEE) is currently an Associate Professor and the Head of the Photonics and Optoelectronics Laboratory, Department of Telecommunications, Faculty of Electrical Engineering and Computer Science, Technical University of Ostrava. He is also a member of the Scientific Council, the Senator of the Academic Chamber of the Senate, a member of the Doctoral and Habilitation Committees, and a Guarantor of bachelor's study programs at the Faculty of Electrical Engineering and Computer Science. During his scientific career, he was the leader or the co-investigator of more than 30 projects and has more than 200 journal articles and conference papers in his research areas. He holds 12 valid Czech patents. His research interests include optical communications and optical wireless communications, photonics, optoelectronics, optical measurements, communications and information engineering, smart sensors, fiber optic sensors, and biomedical engineering. In 2023, he was added to the list of the Top 2% of World Scientists in the field of optoelectronics and photonics (Stanford University Ranking).